

Seminar Report Title

SEMINAR REPORT

**SUBMITTED IN PARTIAL FULFILLMENT OF THE
REQUIREMENTS FOR THE AWARD OF DEGREE OF**

BACHELOR OF TECHNOLOGY

in

ELECTRICAL AND ELECTRONICS ENGINEERING

of

APJ Abdul Kalam Technological University

by

Student Name

Univ. Reg.No. University Register Number



(AN ISO 9001:2008 CERTIFIED INSTITUTION)

Department of Branch of Engineering

Vidya Academy of Science & Technology

Thalakkottukara, Thrissur - 680 501

(<http://www.vidyaacademy.ac.in>)

November 2018

Department of Branch of Engineering
Vidya Academy of Science & Technology

Thalakkottukara, Thrissur - 680 501

(<http://www.vidyaacademy.ac.in>)



(AN ISO 9001:2008 CERTIFIED INSTITUTION)

Certificate

This is to certify that the seminar report titled “**Seminar Report Title**” is a bonafide record of the work carried out by **Student Name (Univ. Reg.No. University Register Number)** of Vidya Academy of Science & Technology, Thalakkottukara, Thrissur - 680 501 in partial fulfillment of the requirements for the award of **Degree of Bachelor of Technology in Electrical and Electronics Engineering** of **APJ Abdul Kalam Technological University**, during the academic year 2020-2021.

Seminar Guide/Supervisor

Head of Department

Guide Name

HoD Name

Asst. Prof., Dept. of EEE

Prof., Dept. of ***

Acknowledgement

I wish to record my indebtedness and thankfulness to all those who helped me prepare this report titled “**Seminar Report Title**” and present it in a satisfactory way.

First and foremost I thank God Almighty for His providence and for being the guiding light throughout the seminar.

I would like to thank my guide **Guide Name**, Asst. Prof., of Branch of Engineering Dept. for providing critical inputs in the preparation of this report. I also thank all other faculty members in our department for their guidance.

I am thankful to **HoD Name**, Head of Branch of Engineering Department, and our Principal **Principal Name**, for their sole co-operation.

Finally, I would like to extend my sincere gratitude to friends who have always been helpful, in preparing and presenting the report and in the discussion following the presentation.

Student Name

Reg. No. University Register Number

Seventh Semester B.Tech (2017 Admissions)

Vidya Academy of Science & Technology

Thrissur - 680 501.

November 2018

Abstract

Copy your Abstract of the seminar here . . .

Contents

ACKNOWLEDGEMENT	i
ABSTRACT	ii
LIST OF FIGURES	iii
LIST OF TABLES	iv
LIST OF SYMBOLS AND ABBREVIATIONS	v
1 INTRODUCTION	1
1.1 General	1
1.2 Objectives of the Work	2
1.3 Outline of Report	2
2 TOPOLOGIES	3
2.1 PRIMARY SIDE SWITCH TOPOLOGY	3
2.2 SECONDARY SIDE SWITCH TOPOLOGY	3
2.3 SECONDARY SIDE SWITCH TOPOLOGY	4
3 RESULTS OF THE SETUP	5
4 CONCLUSION	7
BIBLIOGRAPHY	8
APPENDIX	9

List of Figures

1.1	Resonance based inertial Electromagnetic Microgenerator	1
1.2	Resonance based inertial Electromagnetic Microgenerator	2
2.1	Operation modes of the split capacitor topology converter	4
2.2	Circuit A, B and C	4

List of Tables

3.1	Table Name	6
-----	----------------------	---

List of Symbols and Abbreviations

VAST	Vidya Academy of Science and Technology
A_i	Area of the i^{th} component
DC	Direct current electricity
DSO	Digital Storage Oscilloscope
FBI	Full Bridge Inverter

Chapter 1

INTRODUCTION

Give some intro abt this chapter

1.1 General

Give some introduction abt the project, maximum 1 or 2 pages . . .

Electrical engineering is a field of engineering that generally deals with the study and application of electricity, electronics, and electromagnetism. This field first became an identifiable occupation in the latter half of the 19th century after commercialization of the electric telegraph, the telephone, and Fig. 1.2

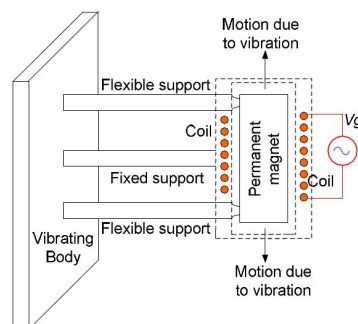


Figure 1.1: Resonance based inertial Electromagnetic Microgenerator

electric power distribution and use.[1] Photovoltaic (PV) power supplied to the system is gaining more and more visibility. [3]

Photovoltaic (PV) power supplied to the system is gaining more and more visibility Solid-state inverters have shown for putting PV systems now. [2]

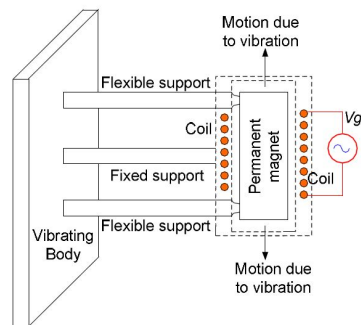


Figure 1.2: Resonance based inertial Electromagnetic Microgenerator

1.2 Objectives of the Work

The concept of micro-inverter (also known as a module integrated converter / inverter) has . . .

A plug-in DMRC system under consideration, where $R(z)$ is the reference input, $Y(z)$ is the output, $E(z) = R(z) - Y(z)$ is the tracking error, $D(z)$ is the disturbance, $G_c(z)$ is the conventional feedback controller, $G_s(z)$ is the plant, $G_{dr}(z)$ is . . .

1.3 Outline of Report

First Chapter contains Second chapter contains . . .

Chapter 2

TOPOLOGIES

Give some intro abt this chapter

A plug-in DMRC system under consideration, where $R(z)$ is the reference input, $Y(z)$ is the output, . . .

2.1 PRIMARY SIDE SWITCH TOPOLOGY

A plug-in DMRC system under consideration, where $R(z)$ is the reference input, $Y(z)$ is the output, $E(z) = R(z) - Y(z)$ is the tracking error, $D(z)$ is the disturbance, $G_c(z)$ is the conventional feedback controller, $G_s(z)$ is the plant, $G_{dr}(z)$ is a feedforward plug-in [3].

2.2 SECONDARY SIDE SWITCH TOPOLOGY

A plug-in DMRC system under consideration, where $R(z)$ is the reference input, $Y(z)$ is the output, $E(z) = R(z) - Y(z)$ is the tracking error, $D(z)$ is the disturbance,

A plug-in DMRC system under consideration, where $R(z)$ is the reference input, $Y(z)$ is the output, $E(z) = R(z) - Y(z)$

$$d_f T_s = i_{pk} / m_2 = i_{pk} L_1 / (V_0 - v_{ik}) \quad (2.1)$$

During this switching cycle, the energy (E_k) transferred from the input to the output can be obtained as:

$$E_k = v_{ik} \cdot i_{pk} \cdot T_s (D + d_f) / 2 \quad (2.2)$$

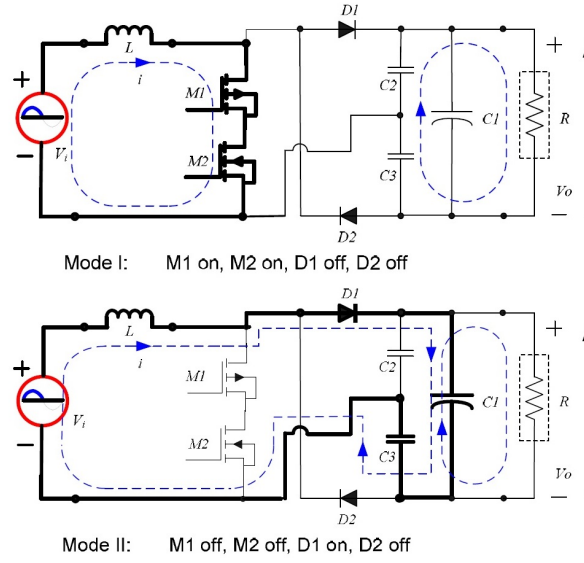


Figure 2.1: Operation modes of the split capacitor topology converter

2.3 SECONDARY SIDE SWITCH TOPOLOGY

A plug-in DMRC system under consideration, where $R(z)$ is the reference input, $Y(z)$ is the output, . . .

For equ..

$$d_f T_s = i_{pk} / m_2 = i_{pk} L_1 / (V_0 - v_{ik}) \quad (2.3)$$

During this switching cycle, the energy (E_k) transferred from the input to the output can be obtained as:

$$E_k = v_{ik} \cdot i_{pk} \cdot T_s (D + d_f) / 2 \quad (2.4)$$

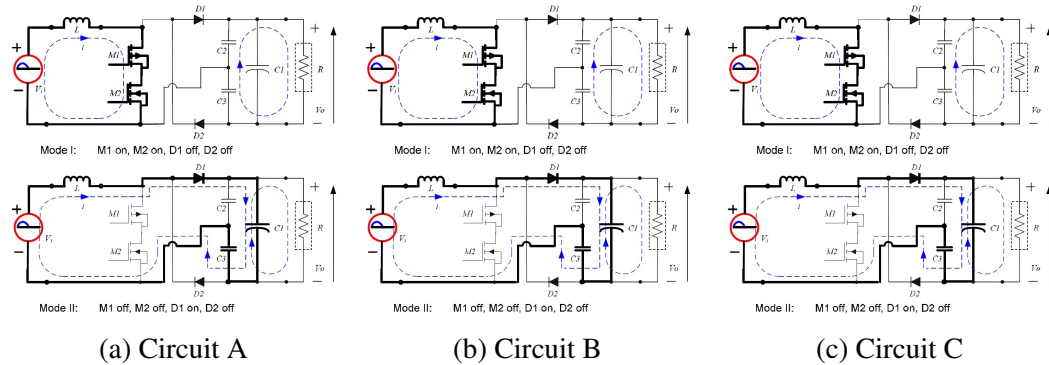


Figure 2.2: Circuit A, B and C

Chapter 3

RESULTS OF THE SETUP

A plug-in DMRC system under consideration, where $R(z)$ is the reference input, $Y(z)$ is the output, $E(z) = R(z) - Y(z)$ is the tracking error, $D(z)$ is the disturbance, $\hat{P} G_c(z)$ is the conventional . . .

To use bullets

- Presented
- Paper
- Presented
- Paper

General, a micro-inverter PV is often provided by a low voltage solar panel, which requires a high voltage lift ratio to produce the desired AC output .

- Presented
- Paper
 - Presented
 - Paper
- Presented
- Paper

Inverter has become a future trend for single phase photovoltaic (PV) power. In general, a micro-inverter PV is often provided by a low voltage solar panel . . .

To use 1,2,3, numbers

1. prepare a source file with the extension "tex"
2. Compile it with \LaTeX to produce a "dvi" file
3. Print the document using a "dvi" driver

For making a table . . .

Planet	Diameter(km)
Mercury	4878
Pluto	2274
Mercury	4878
Pluto	2274
Mercury	4878
Pluto	2274
Mercury	4878
Pluto	2274

Table 3.1: Table Name

Chapter 4

CONCLUSION

Controller, $G_f(z)$ is a filter to obtain a stable overall closed-loop system, and $Q(z)$ is a lowpass filter to enhance the robustness of the overall system at the cost of imperfect elimination of high-frequency errors. The feedback controller $G_c(z)$ is chosen so that the transfer function.

Bibliography

- [1] Suman Dwari, Leila Parsa, and Rohan Dayal, Design and Implementation of a Direct ACDC Boost Converter for Low-Voltage Energy Harvesting, *IEEE Transactions on Industrial Electronics*, Vol. 58, No. 6, June 2011, pp. 2387-2396.
- [2] Suman Dwari and Leila Parsa, "Efficient Low Voltage Direct AC/DC Converters for Selfpowered Wireless Sensor Nodes and Mobile Electronics, *Telecommunications Energy Conference*, Intelec Sept. 2008.
- [3] Suman Dwari and Leila Parsa,, "An Efficient ACDC Step-Up Converter for Low-Voltage Energy Harvesting," *IEEE Transactions on Power Electronics*, Vol. 25, No. 8, August 2010, pp. 2188-2199.

APPENDIX

- Reference Paper of the Seminar
- PPT of the Seminar

High Sensitivity of Temperature Sensor Based on Ultracompact Photonics Crystal Fibers

Volume 6, Number 6, December 2014

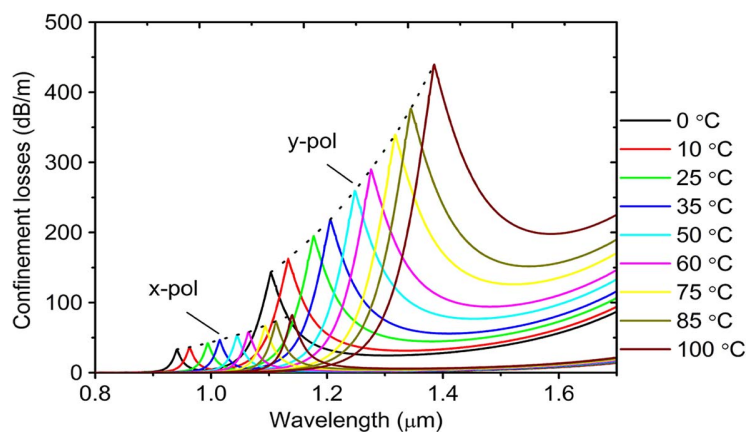
Hailiang Chen, Student Member, IEEE

Shuguang Li

Jianshe Li

Ying Han

Yidong Wu



DOI: 10.1109/JPHOT.2014.2366157

1943-0655 © 2014 IEEE

High Sensitivity of Temperature Sensor Based on Ultracompact Photonics Crystal Fibers

Hailiang Chen, *Student Member, IEEE*, Shuguang Li, Jianshe Li, Ying Han, and Yidong Wu

State Key Laboratory of Metastable Materials Science and Technology, College of Science, Yanshan University, Qinhuangdao 066004, China

DOI: 10.1109/JPHOT.2014.2366157

1943-0655 © 2014 IEEE. Translations and content mining are permitted for academic research only. Personal use is also permitted, but republication/redistribution requires IEEE permission. See http://www.ieee.org/publications_standards/publications/rights/index.html for more information.

Manuscript received August 25, 2014; revised October 11, 2014; accepted October 15, 2014. Date of publication October 31, 2014; date of current version November 11, 2014. This work was supported in part by the National Natural Science Foundation of China under Grant 61178026 and in part by the Natural Science Foundation of Hebei Province, China, under Grant E2012203035. Corresponding author: S. Li (e-mail: shuguangli@ysu.edu.cn).

Abstract: A temperature sensor with high sensitivity based on ultracompact photonics crystal fibers is proposed and analyzed by the finite-element method. The temperature-sensitive materials are injected into one cladding air hole, which shows high confinement loss and works as a defect core. As the phase-matched condition is satisfied, the power in the transferring core couples to the defect core. The temperature sensitivity and figure of merit reach to $2.82 \text{ nm}/^\circ\text{C}$, $0.105/^\circ\text{C}$ and $1.99 \text{ nm}/^\circ\text{C}$, $0.048/^\circ\text{C}$, for the y-polarized and x-polarized directions, respectively, which are one to two orders of magnitude better than other reported sensors. The performance characteristics can be further improved by optimizing the structure parameters and infilling materials.

Index Terms: Photonics crystal fibers, temperature sensitive materials, temperature sensor.

1. Introduction

The temperature sensor with compact structure and easy remote control is an important factor in the remote sensors and communication systems. Optical fibers, exhibiting high sensitivity, immunity to electromagnetic wave, corrosion resistance and easy remote control, have been utilized as the sensor medium in the past [1]–[3]. Grobner [4] reported a sapphire fiber Bragg grating sensor with sensitivity of $25 \text{ pm}/^\circ\text{C}$. Photonics crystal fibers (PCFs), benefit to its holey structure, are infiltrated with various functional materials to fabricate sensors. Lee [5] proposed a polymer filled hollow-core PCF temperature sensor showing high sensitivity of $-1.7 \text{ nm}/^\circ\text{C}$. Contrast to the difficult fusion splicing of polymer, it is relatively easier to fill the liquid into the air holes. Qiu [6] demonstrated an isopropanol-sealed PCF temperature sensor with sensitivity of $-166 \text{ pm}/^\circ\text{C}$. The side-polished microstructured optical fiber enhanced the effective area of the infilling material and a temperature sensitivity of $0.38 \text{ dB}/^\circ\text{C}$ is obtained [7]. Based on the intense surface plasmon resonance, the metal wires and films were injected into the air holes to get a high temperature sensitivity of $720 \text{ pm}/^\circ\text{C}$ [8].

In favor of high spectra acutance, various optical interferometers have been employed in sensing devices [9]–[11]. A high sensitive temperature sensors based on fiber loop mirror

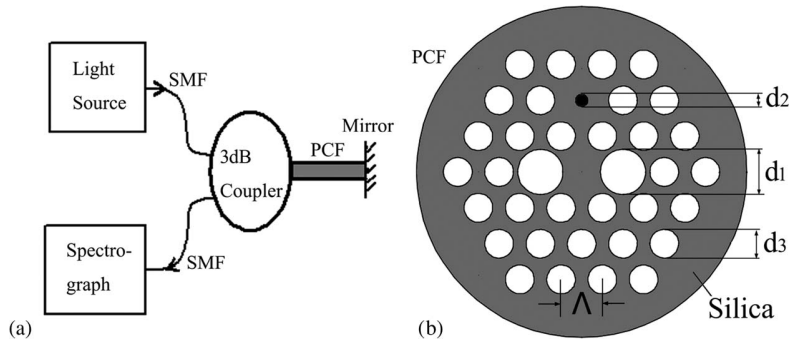


Fig. 1. (a) The schematic of temperature sensor system and (b) cross section of TSM-PCF. The black air hole is infiltrated with temperature sensitive materials.

interferometers have been reported with a high sensitivity of about $0.94 \text{ nm}/^\circ\text{C}$ [12]. Zhang [13] proposed a fiber optic extrinsic Fabry-Perot interferometer based on polymer-filled glass capillary with high sensitivity of $5.2 \text{ nm}/^\circ\text{C}$. Limited to the free spectral range, however, the interferometers usually exhibit a narrow measurement range from 15°C to 22°C reported in [13].

In this paper, we designed a temperature sensor based on an ultra compact PCF. The temperature sensitive materials are supposed to be injected into one cladding air hole to form a defect core. As the phase matched condition is satisfied, the power in the transferring core couples to the defect core and the confinement losses increase remarkably. The defect core is labeled at the neighborhood of the transferring core and thus the couple can be complete. The designed temperature sensor avoiding transferring in high loss materials, showing ultra compact structure, low cost, high linearity, high sensitivity and figure of merit (FOM), are competitive for application in temperature measurement devices.

2. The Novel Design of Polarization Splitter

Fig. 1(a) shows the schematic of the designed temperature sensor system. The light source exports stable, continuous and broadband lights. The upper single mode fiber (SMF) connects the light source and the input port of the photonics crystal fiber which is infiltrated with temperature sensitive materials (TSM-PCF). The below SMF is utilized to connect the output port of the TSM-PCF and the spectrograph. A reflex mirror is located at the end of the TSM-PCF to increase the effective transferring distance. Fig. 1(b) depicts the cross section of the TSM-PCF. Two big air holes with diameters of d_1 are placed at the left and right of the core to achieve birefringence effect. The black air hole with diameters of d_2 is infiltrated with temperature sensitive materials. The rest air holes with diameters of d_3 are benefit to confine the power in the cores. The adjacent air holes pitch is labeled by Λ .

The background material of the TSM-PCF is fused silica and the dispersion relationship of which can be expressed by the Sellmeier equation [14]

$$n^2(\lambda, T) = (1.31552 + 6.90754 \times 10^{-6} T) + \frac{(0.788404 + 23.5835 \times 10^{-6} T)\lambda^2}{\lambda^2 - (0.0110199 + 0.584758 \times 10^{-6} T)} + \frac{(0.91316 + 0.548368 \times 10^{-6} T)\lambda^2}{\lambda^2 - 100} \quad (1)$$

where T is the temperature in Celsius, and λ is the free space wavelength in microns. Many liquids such as alcohol, methylbenzene, chloroform, and index-matching fluids exhibit high refractive index-temperature sensitive coefficient of about $-4 \times 10^{-4}/^\circ\text{C}$. In this paper, the refractive index of the temperature sensitive materials is designed as

$$n_{\text{TSM}} = 1.37 - 4 \times 10^{-4} T \quad (2)$$

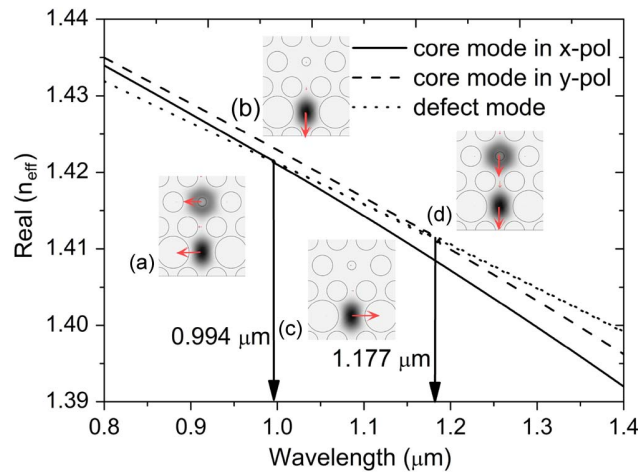


Fig. 2. Effective refractive indices of core modes and defect modes relying on wavelengths. The inserts show the electrical field profile at $0.994 \mu\text{m}$ in (a) the x-polarized direction and (b) the y-polarized direction and at $1.177 \mu\text{m}$ in (c) the x-polarized direction and (d) the y-polarized direction, respectively. The parameters are $d_1 = 2.2 \mu\text{m}$, $d_2 = 0.6 \mu\text{m}$, $d_3 = 1.4 \mu\text{m}$, $\Lambda = 2.0 \mu\text{m}$, and $T = 25^\circ\text{C}$.

where n_{TSM} is 1.37 at 0°C . The actual measurement range is influenced by the freezing point and boiling point of the infilling liquid.

3. Simulation Results and Analysis

The FEM providing high accuracy and flexible triangular meshes was implemented to characterize the performance of the TSM-PCF. The scattering boundary conditions and a perfect matched layer were employed in the simulation process. As the refractive index of the temperature sensitive materials is less than silica, the temperature sensitive materials infilled air hole shows high confinement losses and works like a defect core. Fig. 2 shows the effective refractive indices of the core modes and defect modes. It is clear to see that the refractive indices of defect modes have intersections with the core modes at $0.994 \mu\text{m}$ in the x-polarized direction and $1.177 \mu\text{m}$ in the y-polarized direction. At the intersection point, the resonance appears and the energy couples between core modes and defect modes which can be clarified by the inserts in Fig. 2.

Fig. 3 demonstrates the confinement losses spectra of core modes and defect modes as a function of wavelength. At the intersection points, the confinement losses of core modes experience rapid increases and meanwhile the confinement losses of defect modes show fast decreases. It also should be noted that the confinement losses of core modes and defect modes are equal at phase matched points. It indicates that the imaginary parts of effective refractive indices are identical for core modes and defect modes. The couple between core modes and defect modes is complete which is benefit to obtain a high detection signal.

With the temperature increasing, the refractive index of the temperature sensitive material gets smaller. Thus, the refractive indices of defect modes become smaller, while the refractive indices of core modes have no significant variation. It results in a red shift of the phase matched points. Fig. 4 depicts the confinement losses spectra of core modes at different temperatures changing from 0°C to 100°C . The intensity of confinement losses at phase matched points increases as temperature increasing. It also should be pointed out that the couples between core modes and defect modes are always complete as temperatures changing from 0°C to 100°C .

Fig. 5 shows the resonant wavelengths as a function of temperature in x-polarized and y-polarized directions. The peak wavelengths increases linearly as temperature increasing from 0°C to 100°C , which is very important for application. The sensitivity of the designed temperature

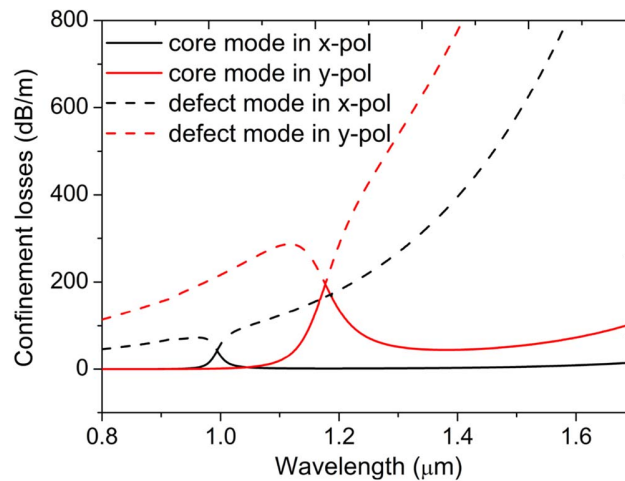


Fig. 3. Confinement losses spectra of core modes and defect modes relying on wavelengths.

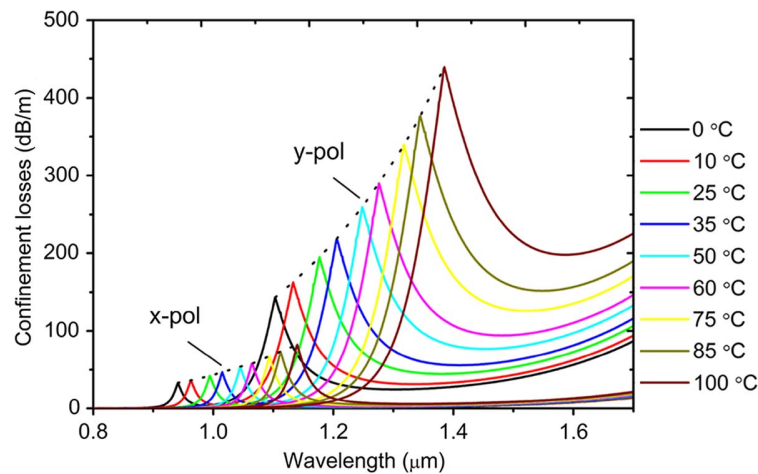


Fig. 4. Confinement losses spectra of core modes under different temperatures.

sensor is defined by $S = d\lambda_{\text{peak}}/dT$. It can be concluded from the fit lines that the sensitivity is 1.99 nm/°C for the x-polarized direction and 2.82 nm/°C for the y-polarized direction.

The spectra width and signal to noise ratio (SNR) both contribute to a better detection limit. This can be demonstrated by figure of merit (FOM). The FOM is defined by $\text{FOM} = S/\text{FWHM}$, where FWHM is the full width at half-maximum. Fig. 6 shows the FOM curves as a function of temperature. It reviews that FOM decreases linearly as the temperature increasing. This is mainly depended on the fact that the spectra width gets broadened as temperature increasing. The FOM is 0.0467 °C⁻¹ for x-polarized direction and 0.10238 °C⁻¹ for y-polarized direction at 0 °C.

The performance characteristics of the designed temperature sensor are influenced by the structure parameters of the PCF. It is well known that the mode's refractive index is mainly affected by the air holes of first ring [15]. As the diameters of d_2 increasing from 0.6 μm to 0.62 μm, the refractive index of the defect mode decreases. Meanwhile, the diameters of d_2 have no significant effect on the refractive indices of core modes. Thus, the phase matched points experience a red shift and the loss peaks move forward to the longer wavelengths as can be seen in Fig. 7. The decreasing of refractive index of defect mode also results in the increasing of resonant wavelengths displacement from 22 nm to 23 nm for the x-polarized

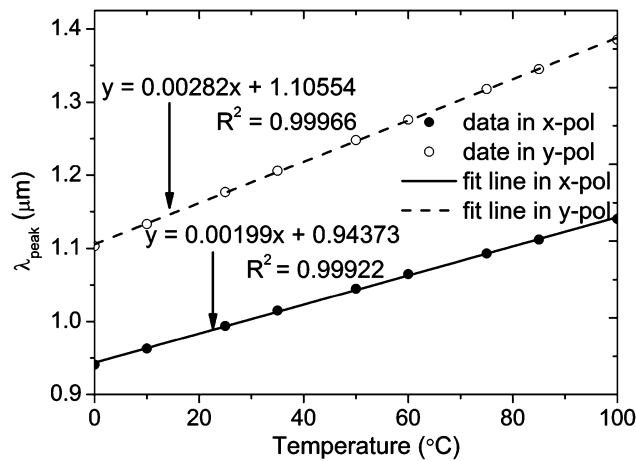


Fig. 5. The resonant wavelengths as a function of temperature in the x-polarized and y-polarized directions.

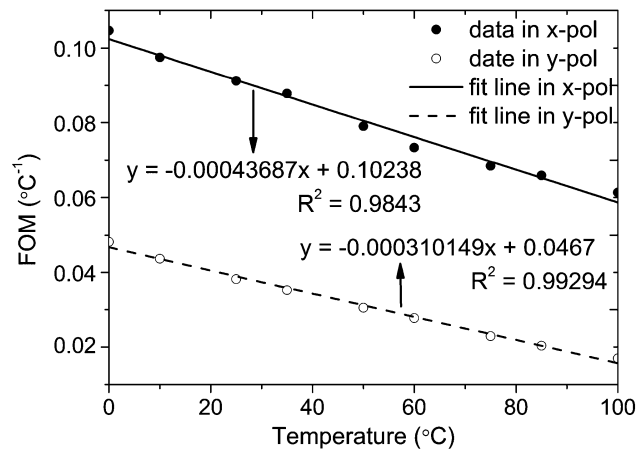


Fig. 6. The figures of merit as a function of temperature in the x-polarized and y-polarized directions.

direction and from 30 nm to 31 nm for the y-polarized direction, as temperature increasing from 0 °C to 10 °C. It indicates that the sensitivity of the temperature sensor can be improved by the increasing of d_2 . The diameters of d_1 have vital influence on the refractive indices of core modes and faint influence on the refractive index of defect mode. The diameters of d_3 and adjacent air holes pitch simultaneously affect the refractive indices of core modes and defect mode. Thus, the resonant wavelength displacement and sensitivity can be further improved by adjusting the PCF structure parameters.

4. Conclusion

A high-sensitivity temperature sensor based on ultra compact PCFs is proposed. The temperature sensitive materials are injected into one cladding air hole and function as a defect core. The defect core is localized at the neighborhood of the transferring core to ensure that the couples between core modes and defect modes are complete. The sensitivity and FOM can reach to 1.99 nm/°C, 0.048/°C for the x-polarized direction and 2.82 nm/°C, 0.105/°C for the y-polarized direction, respectively. Both of the two polarized directions can be used to detect temperature

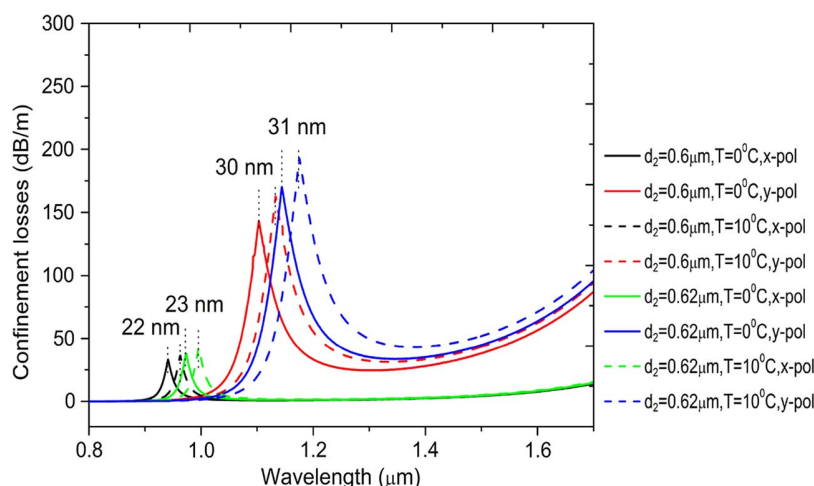


Fig. 7. Confinement losses spectra under different diameters of d_2 .

and even self-correction. The performance characteristics can be further improved by optimizing the PCF structure parameters. The temperature sensitive materials with higher index-temperature coefficient also are very useful to enhance the performance characteristics. The designed temperature sensor showing perfect performance characteristics is suitable for the application in temperature measurement.

Acknowledgement

The authors wish to thank the anonymous reviewers for their valuable suggestions.

References

- [1] S. K. Srivastava, R. Verma, and B. D. Gupta, "Surface plasmon resonance based fiber optic sensor for the detection of low water content in ethanol," *Sens. Actuators B, Chem.*, vol. 153, no. 1, pp. 194–198, Mar. 2011.
- [2] P. S. Reddy *et al.*, "Method for enhancing and controlling temperature sensitivity of fiber Bragg grating sensor based on two bimetallic strips," *IEEE Photon. J.*, vol. 4, no. 3, pp. 1035–1041, Jun. 2012.
- [3] P. Zu *et al.*, "Enhancement of the sensitivity of magneto-optical fiber sensor by magnifying the birefringence of magnetic fluid film with Lott-Sagnac interferometer," *Sens. Actuators B, Chem.*, vol. 191, pp. 19–23, Feb. 2014.
- [4] D. Grobnc, S. J. Mihailov, C. W. Smelser, and H. Ding, "Sapphire fiber Bragg grating sensor made using femtosecond laser radiation for ultrahigh temperature applications," *IEEE Photon. Technol. Lett.*, vol. 16, no. 11, pp. 2505–2507, Nov. 2004.
- [5] C. L. Lee, L. H. Lee, H. E. Hwang, and J. M. Hsu, "Highly sensitive air-gap fiber Fabry–Pérot interferometers based on polymer-filled hollow core fibers," *IEEE Photon. Technol. Lett.*, vol. 24, no. 2, pp. 149–151, Jan. 2012.
- [6] S. J. Qiu, Y. Chen, F. Xu, and Y. Q. Lu, "Temperature sensor based on an isopropanol-sealed photonic crystal fiber in-line interferometer with enhanced refractive index sensitivity," *Opt. Lett.*, vol. 37, no. 5, pp. 863–865, Mar. 2012.
- [7] M. A. Franco, V. A. Serrao, and F. Sircilli, "Side-polished microstructured optical fiber for temperature sensor application," *IEEE Photon. Technol. Lett.*, vol. 19, no. 21, pp. 1738–1740, Nov. 2007.
- [8] Y. Peng, J. Hou, Z. Huang, and Q. Lu, "Temperature sensor based on surface plasmon resonance within selectively coated photonic crystal fiber," *Appl. Opt.*, vol. 51, no. 26, pp. 6361–6367, Sep. 2012.
- [9] P. Kozma, A. Hmori, S. Kurunczi, K. Cottier, and R. Horvath, "Grating coupled optical waveguide interferometer for label-free biosensing," *Sens. Actuators B, Chem.*, vol. 155, no. 2, pp. 446–450, Jul. 2011.
- [10] W. Chen *et al.*, "Highly sensitive torsion sensor based on Sagnac interferometer using side-leakage photonic crystal fiber," *IEEE Photon. Technol. Lett.*, vol. 23, no. 21, pp. 1639–1641, Nov. 2011.
- [11] K. Takahashi *et al.*, "Surface stress sensor using MEMS-based Fabry–Pérot interferometer for label-free biosensing," *Sens. Actuators B, Chem.*, vol. 188, pp. 393–399, Nov. 2013.
- [12] Y. G. Liu *et al.*, "High-birefringence fiber loop mirrors and their applications as sensors," *Appl. Opt.*, vol. 44, no. 12, pp. 2382–2390, Apr. 2005.
- [13] G. Zhang, M. Yang, and M. Wang, "Large temperature sensitivity of fiber-optic extrinsic Fabry–Pérot interferometer based on polymer-filled glass capillary," *Opt. Fiber Technol.*, vol. 19, no. 6, pp. 618–622, Dec. 2013.
- [14] G. Ghosh, M. Endo, and T. Iwasaki, "Temperature-dependent Sellmeier coefficients and chromatic dispersions for some optical fiber glasses," *J. Lightw. Technol.*, vol. 12, no. 8, pp. 1338–1342, Aug. 1994.
- [15] K. Saitoh and M. Koshiba, "Numerical modeling of photonic crystal fibers," *J. Lightw. Technol.*, vol. 23, no. 11, pp. 3580–3590, Nov. 2005.



Title Slide

Name



Slide 1



Slide 2



Slide 3



Slide 4



Slide 5





Department of Branch of Engineering
Vidya Academy of Science & Technology
Thalakkottukara, Thrissur - 680 501
(<http://www.vidyaacademy.ac.in>)